Impacts of the Pacific Meridional Mode on North Atlantic Tropical Cyclones Making U.S. Landfall

Wei Zhang[1,*], Gabriele Villarini[1], Gabriel A. Vecchi[2,3], Hiroyuki Murakami[2,3]

[1]IIHR-Hydroscience & Engineering, The University of Iowa, Iowa City, Iowa, USA

[2]National Oceanic and Atmospheric Administration/Geophysical Fluid Dynamics Laboratory, Princeton, NJ, USA

[3]Atmospheric and Oceanic Sciences Program, Princeton University, Princeton, NJ, USA

To be submitted to Climate Dynamics

*Corresponding author:
Wei Zhang, Ph.D.
IIHR-Hydroscience & Engineering, The University of Iowa, Iowa City, Iowa, USA
Email: wei-zhang-3@uiowa.edu

Abstract

This study examines the impacts of the Pacific Meridional Mode (PMM) on North Atlantic tropical cyclones (TCs) making landfall along the coastal United States, and provides insights on the underling physical mechanisms using observations and model simulations. There is a statistically significant time-lagged association between Spring PMM and the August-October U.S. landfalling TCs. Specifically, the positive (negative) Spring PMM events tend to be followed by fewer (more) TCs affecting the coastal United States, especially over the Gulf of Mexico and Florida. This lagged association is mainly caused by the lagged impacts of PMM on the El Niño Southern Oscillation (ENSO), and the subsequent impacts of ENSO on TC frequency and landfall. Positive (negative) PMM events are largely followed by El Niño (La Niña) events, which lead to less (more) TC geneses close to the U.S. coast (i.e., the Gulf of Mexico and the Caribbean Sea); this also leads to easterly (westerly) steering flow in the vicinity of the U.S. coast, which are unfavorable (favorable) for TC landfall across the Gulf of Mexico and Florida. Perturbation simulations with the state-of-the-art Geophysical Fluid Dynamics Laboratory (GFDL) Forecast-oriented Low Ocean Resolution Version of CM2.5 (FLOR) supports the linkage between PMM and TC landfall activity. The time-lagged impacts of Spring PMM on TC landfalling activity results in a new predictor to forecast seasonal TC landfall activity over the U.S. coast, especially over the Gulf of Mexico and Florida.

1. Introduction

North Atlantic tropical cyclones (TCs) are one of the costliest and most catastrophic natural hazards affecting the United States (e.g., Pielke Jr et al. 2008; Smith and Katz 2013). TCs cause severe damages to the coastal and inland regions during or after landfall (e.g., Pielke Jr and Landsea 1999; Pielke Jr et al. 2008), with significant impacts due to strong winds, heavy rainfall, flooding, and storm surge. Despite the significant societal and economic impacts associated with these storms, the prediction of TC landfall is still a very challenging problem (e.g., Marks and Shay 1998; Saunders and Lea 2005; Elsner and Jagger 2006; Vecchi and Villarini 2014; Vecchi et al. 2014; Murakami et al. 2016). It is therefore of crucial importance to better understand what controls the frequency and variability of landfalling TCs in terms of climate processes, which in turn can lay the foundation for better predictions.

In general, the U.S. TC landfall activity tends to be suppressed (enhanced) during El Niño (La Niña) events (e.g., Bove et al. 1998; Pielke Jr and Landsea 1999; Elsner 2003; Elsner and Jagger 2006; Smith et al. 2007) because of the modulation of the vertical wind shear and steering flow in the North Atlantic (e.g., Bove et al. 1998; Klotzbach 2011). After the identification of the central Pacific El Niño/Warm Pool El Niño (CP El Niño; e.g., Ashok et al. 2007; Weng et al. 2007; Kug et al. 2009), several studies have been devoted to the analysis of whether, how and to what extent CP El Niño modulates TC landfall (Kim et al. 2010; Lee et al. 2010; Larson et al. 2012; Wang et al. 2014; Patricola et al. 2016). In addition to ENSO, there have been other climate modes that have been found to be related to the frequency and tracking of U.S. landfalling TCs. For instance, the Atlantic warm pool, which is a large body of warm water covering the Gulf of Mexico, the Caribbean Sea, and the western tropical North Atlantic, has been found to modulate TC landfall rate by changing both genesis locations and steering flow (Wang and Lee 2007; Wang et al. 2008,

2011). In particular, large (small) values of the Atlantic warm pool tend to produce steering flow unfavorable (favorable) for TC landfall over the U.S. coast; this then leads to a smaller (larger) number of TCs in the main development region (MDR) than the climatology in the presence of a large (small) Atlantic warm pool (Wang and Lee 2007; Wang et al. 2008, 2011). Moreover, the Atlantic Multidecadal Oscillation (AMO) can also influence the modulation of ENSO on TC landfall (Klotzbach 2011); while the North Atlantic Oscillation (NAO) has been found to affect TC landfall by changing the steering flow and subtropical ridge (e.g., Xie et al. 2005; Kossin et al. 2010; Villarini et al. 2011).

In addition to these climate modes, there has been recent work relating ENSO and the Pacific Meridional Mode (PMM), which is defined as the first Maximum Covariance Analysis (MCA) of sea surface temperature (SST) and the zonal and meridional components of the 10m wind field (Chiang and Vimont 2004). PMM acts effectively as a conduit through which the extra-tropical atmosphere influences ENSO (e.g., Anderson 2003, 2004; Chang et al. 2007; Boschat et al. 2013). For example, the North Pacific Oscillation (NPO)/Victoria mode can affect the onset of El Niño/La Niña in which PMM acts as a bridge by the seasonal footprinting mechanism (Vimont et al. 2001, 2003; Chiang and Vimont 2004; Ding et al. 2015), indicating that PMM is closely linked with the development of ENSO (Chang et al. 2007; Zhang et al. 2009a, b; Kim et al. 2012; Pegion and Alexander 2013; Larson and Kirtman 2014; Di Lorenzo et al. 2015; Ding et al. 2015; Lin et al. 2015). Positive (negative) values of PMM that peaks in spring are largely followed by El Niño (La Niña) events (Chang et al. 2007; Zhang et al. 2009a, b; Larson and Kirtman 2014). In terms of TC activity, for instance, PMM strongly modulates the occurrence of typhoons in the western North Pacific by mediating vertical wind shear and this association is verified in both observations and long control experiments using a coupled climate model (Zhang et al. 2016).

96 The association between PMM and ENSO, and that between ENSO and TC landfall suggests
97 that PMM may influence TC landfall. The goal of this study is, therefore, to examine the role
98 played by PMM via ENSO in controlling the frequency and tracking of U.S. landfalling TCs. By
99 advancing our understanding of the physical processes controlling U.S. landfalling activity, we
100 will provide basic information that can lead to the improved seasonal predictions of these storms.
101 This paper is organized as follows. Section 2 presents the data and methodology, while Section
102 3 discusses the results based on observations and simulations. Section 4 includes the discussion
103 and summarizes the main conclusions.
104

105 ## 2. Data and Methodology

106 The information about North Atlantic TCs is based on latitude, longitude and time of
107 occurrence of TC data are obtained from the National Oceanic and Atmospheric Administration's
108 (NOAA) National Hurricane Center's best-track database (HURDAT2; Landsea and Franklin 2013)
109 available for the period 1851-2015. We use the Met Office Hadley Center (HadISST, version 1.1;
110 Rayner et al. 2003) as reference SST data, while the atmospheric variables are obtained from the
111 National Centers for Environmental Prediction (NCEP)/National Center for Atmospheric Research
112 (NCAR) reanalysis project (NCEP-NCAR; Kalnay et al. 1996).
113 We divide the U.S. coastline facing the Gulf of Mexico and the Atlantic Ocean into four main
114 regions (Figure 1): Southwest (Gulf of Mexico), Florida, Southeast and Northeast. We consider as
115 a landfalling TC affecting any of these four regions if the center of circulation of the storm is within
116 300 km from the coastline. Moreover, we focus only on storms that occurred during the August-
117 October months (ASO).
118 Steering flow is used to analyze the environmental flow that leads to the changes in TC tracks.

Steering flow is defined as the deep-layer mean wind fields from 850 hPa to 200 hPa levels (e.g., Chan and Gray 1982; Velden et al. 1992).

The PMM index is calculated following the methodology described in Chiang and Vimont (2004). In calculating it, the seasonal cycle and the linear trend of SST and 10-m wind field are first removed by applying a three-month running mean to the data, and then subtracting the linear fit to the cold tongue index (CTI) (Deser and Wallace 1987) from the spatial grids to remove correlations with El Niño (Chiang and Vimont 2004). The CTI is defined as the SST anomalies averaged over 6°S - 6°N, 180°W - 90°W minus the global mean SST.

We define Niño3.4 index as the SST anomalies over the region 5ºN-5ºS, 120º-170ºW, Nino3 index as the SST anomalies over the region 5ºN-5ºS and 150ºW-90ºW, and Nino4 index as the SST anomalies over the region 5ºN-5ºS, 160ºE-150ºW. SST anomalies are defined with respect to the 1970-2000 base period.

We use the genesis potential index (GPI; Emanuel and Nolan 2004) to examine the potential of TC genesis during the peak seasons when PMM in the previous spring is strongly positive or negative. GPI is defined as:

$$\mathrm{GPI} = |10^5\eta|^{\frac{3}{2}}\left(\frac{\mathcal{H}}{50}\right)^3\left(\frac{\mathrm{v_{pot}}}{70}\right)^3(1+0.1\mathrm{V_{shear}})^{-2} \quad (1)$$

where η is is absolute vorticity at 850 hPa level, $\mathcal{H}$ is the relative humidity at 600 hPa level (unit: percent), $\mathrm{v_{pot}}$ is the potential intensity (unit: $\mathrm{ms^{-1}}$), and $\mathrm{V_{shear}}$ is the vertical wind shear between 850 hPa and 200 hPa levels. GPI involves thermodynamic and dynamic variables that are important for TC genesis. GPI has been widely used to analyze genesis potential in observations and climate models across different basins.

We complement the results from observational and reanalysis datasets using a newly-developed high-resolution coupled climate model for perturbation experiments, the Geophysical

142 Fluid Dynamics Laboratory (GFDL) Forecast-oriented Low Ocean Resolution Version of CM2.5
143 or FLOR (Vecchi et al. 2014). The atmosphere and land components of this model are from the
144 GFDL CM2.5 with a spatial resolution of 50 km × 50 km (Delworth et al. 2012) while its ocean
145 and sea ice components are similar to those in the CM2.1 with a spatial resolution of 1 × 1 degree
146 (Delworth et al. 2006). We use the flux-adjusted version of FLOR (FLOR-FA) (Vecchi et al. 2014).
147 More details about FLOR/FLOR-FA are discussed in Vecchi et al. (2014) and references therein.

148 We perform a set of perturbation experiments to isolate the role of the PMM in forcing the
149 changes in TC activity and tracking. In the control run (CTRL), SST is restored to a repeating
150 annual cycle of the SST climatology in 1860 control run with a ten-day restoring timescale (*tau*).
151 The restoring of SST in the model to the observed estimates is represented by:

152 $$\frac{\mathrm{dSST}}{\mathrm{dt}} = \varsigma + \frac{\mathrm{SSTo} - \mathrm{SST}}{\mathrm{tau}} \quad (2)$$

153 a restoring tendency was applied to the SST tendency as computed in the coupled model (ς) over
154 a restoring time scale *tau* [tau is the constant restoring time scale (e.g., 5-day or 10-day)]; dSST
155 represents the change of SST and dt change of time. SSTo represents a space- and time-dependent
156 array of the observed estimates of SST, while SST is the SST simulated by the model. The larger
157 the tau, the more relaxed the coupling and the weaker the nudging/restoring of SST. A free run
158 with a fully-coupled model has a tau of infinity while Atmospheric Model Intercomparison Project
159 (AMIP) run has a tau of zero. The restoring time scale is set as ten-day because this allows the
160 changes of simulated SST, which is different from AMIP runs in which SST is considered as
161 boundary forcing and cannot be changed. In the perturbation experiment, we prescribe the sum of
162 the annual cycle of SST and the temporally constant SST anomalies associated with the positive
163 PMM patterns (denoted as PPMM) at the ten-day scale. After an initial 100-year spinup, both
164 experiments are integrated for 60 years.

3. Results

The March-May averaged (MAM) PMM index has significant associations with the frequency of ASO TC landfall over the Gulf of Mexico, Florida, and the entire U.S. coast (Table 1). The southern part of the U.S. coast includes the Gulf of Mexico and Florida, which are subject to the largest number of landfalling TCs each year. The correlation coefficient between the MAM PMM index and the number of peak-season (ASO) TCs making landfall over the Gulf of Mexico and Florida for the 1948-2015 is -0.36, and significant at the 0.01 level. However, the correlation coefficients between the PMM index in JJA and ASO and TC landfall activity are much smaller compared to those computed with respect to the MAM PMM. Moreover, we do not find a statistically significant correlation with the other regions.

The time series of the MAM PMM index and the ASO TC landfall frequency are shown in Figure 2. Overall, when the PMM index in spring is positive, there are fewer peak-season TCs making landfall, while the opposite is true for the negative PMM values. For example, the spring PMM index is negative in 1953, 1969, 1971, 1987, 1998, 1999, 2002, 2008 while the peak-season TC landfall over the Gulf of Mexico and Florida is quite active (Figure 2a). Similar results are shown for the entire U.S. coast (Figure 2b). This suggests that there is a marked time-lagged association between PMM and the frequency of landfalling TCs over the Gulf of Mexico, Florida, and the U.S. coast more generally.

Figure 3 illustrates the histogram and fitted Gaussian distribution of MAM PMM indices in the 20 years with the highest and the lowest TC landfall frequency, respectively. Higher/lower landfall frequencies over the Gulf of Mexico, Florida, Gulf of Mexico and Florida combined, and the entire U.S. coast are associated with lower/higher values of the PMM index because of the clear shift in the histogram and fitted distributions (Figure 3). This further supports the lagged

188 linkage between Spring PMM and peak-season TC landfall.

189 Figure 4 depicts the TC density anomalies during the ten years with the largest absolute values
190 of the MAM PMM (Table 2). TC density anomalies are characterized by a dipole mode when the
191 MAM PMM phases are positive (Figure 4a); there is a large positive area of TC density in the
192 eastern North Atlantic while there is a high negative area in the western North Atlantic, Gulf of
193 Mexico, Caribbean region, and the U.S. coast when MAM PMM is positive, suggesting fewer TC
194 landfalls over the U.S. coast, especially over the Gulf of Mexico and Florida (Figure 4a). When
195 MAM PMM is negative, the TC density anomalies are largely opposite to those discussed for the
196 positive MAM PMM (Figure 4b). These findings are consistent with the negative correlation
197 between MAM PMM and ASO TC landfall (Figure 2 and Table 1).

198 Because TC density anomalies are strongly influenced by changes in TC genesis and steering
199 flow (e.g., Wang et al. 2011; Colbert and Soden 2012), we analyze changes in these two quantities
200 to interpret the changes in TC density with respect to the PMM phases. TC genesis anomalies are
201 characterized by negative anomalies in the Gulf of Mexico and western North Atlantic and positive
202 anomalies in the eastern North Pacific when MAM PMM is positive (Figure 5a). This is in good
203 agreement with the negative TC density anomalies along the southern U.S. coast (Figure 4a). When
204 MAM PMM is negative, TC genesis density features positive anomalies in the Gulf of Mexico.
205 Although there is a small region with negative TC genesis anomalies in the Caribbean associated
206 with the negative MAM PMM, TC genesis anomalies are in general positive compared with those
207 during the positive Spring PMM (Figure 5b). Therefore, TC genesis density anomalies during the
208 peak season are mainly consistent with TC density anomalies during the positive or negative MAM
209 PMM phases (Figures 4 and 5).

210 GPI is also consistent with the genesis density anomalies during the different PMM phases.

For example, the GPI anomalies are largely positive (negative) in the Gulf of Mexico, Caribbean and western North Atlantic consistent with the positive (negative) TC genesis anomalies during the negative (positive) MAM PMM (Figure 6). On the other hand, there are differences with respect to GPI and TC genesis in the tropical eastern Atlantic, where stronger GPI anomalies correspond to weaker TC genesis anomalies during the negative PMM phases compared to the positive PMM phase (Figure 6).

4. Physical Mechanisms

4.1 Time-lagged Modulation

The results so far have highlighted the significant time-lagged association between PMM and TC landfall. Here we focus on the physical mechanisms underlying this lagged association. A number of studies have documented that PMM is mostly followed by ENSO events (e.g., Chang et al. 2007; Zhang et al. 2009a, b; Larson and Kirtman 2014). We hypothesize that this lagged association is caused by the PMM-ENSO-TC linkage.

Figure 7 displays that the time series of MAM PMM, and Niño3, Niño3.4 and Niño4 indices averaged over ASO. The correlation coefficients between the PMM (wind) index in the spring and Niño4, Niño3, Niño3.4 in ASO have values of 0.50, 0.42, and 0.48, respectively; these results are statistically significant at the 0.01 level, and consistent with previous findings that PMM is largely followed by ENSO (Chang et al. 2007; Zhang et al. 2009a, b; Larson and Kirtman 2014). The correlation coefficients between the PMM (SST) index in the spring and Niño4, Niño3, Niño3.4 in ASO are similar to those obtained for the PMM (wind) index shown above. The correlation between PMM and Niño4 is higher than those between PMM and Niño3 and Niño3.4, indicating that the PMM may have a slightly higher chance to be followed by the central Pacific El Niño (El

234 Niño Modoki) than by the eastern Pacific El Niño, at least based on the observations.

235 To further substantiate these statistical results, we select the ten years with the strongest
236 positive and the ten years with the strongest negative MAM PMM (Table 2). We composite the
237 SST and steering flow anomalies in MAM, JJA, ASO, and OND. During the positive MAM PMM,
238 the typical PMM mode with positive (negative) SST anomalies in its northwestern (southeastern)
239 part is very strong, while the steering flow in the Atlantic and U.S. sector is negligible along or
240 close to the U.S. coast (Figure 8a). During JJA, the strong positive SST anomalies in the
241 northwestern part of the PMM pattern propagate southeastward towards the tropical Central
242 Pacific. Accompanying this, there are strong northwesterly steering flow anomalies along the U.S.
243 coast (Figure 8b). During ASO (i.e., peak TC season), the positive SST anomalies have moved
244 further southeastward in the tropical central and eastern Pacific and the steering flow anomalies
245 are stronger than in the previous months (Figure 8c). Such steering flow pattern is detrimental to
246 the TC landfall over the U.S. coast: these results provide a mechanism to understand why PMM
247 in the spring impacts TC landfalling activity in the United States. Finally, during OND, an El Niño-
248 like pattern in the tropics develops (Figure 8d).

249 The years characterized by a strongly negative MAM PMM present patterns that are largely
250 the opposite of what described for the positive years. During the positive MAM PMM, there are
251 warm (cool) SST anomalies in the southeastern (northwestern) portion of the tropical and
252 subtropical eastern Pacific (Figure 9a). There is also an anomalous easterly steering flow over the
253 southeastern and northeastern part of the U.S. coast, while there is westerly flow over Florida and
254 the Caribbean regions (Figure 9a). During JJA, the cooling moves equatorward, while the warming
255 diminishes in the southeastern part, in contrast to what observed in MAM. The anomalous steering
256 flow over Florida and the Caribbean changes from westerly to easterly (Figure 9b). During ASO,

the warming in the southeastern part almost disappears, while a La Niña-like pattern develops in the tropical central and eastern Pacific (Figure 9c). Corresponding to this SST pattern, the anomalous easterly steering flow tends to steer TCs to make landfall over the coastal regions (Figure 9c). The propagation of SST warming from the subtropical eastern Pacific to the tropics is supported by the wind-evaporation-SST (WES) feedback associated with thermodynamic air-sea coupling (e.g., Xie and Philander 1994; Chang et al. 1997; Chiang and Bitz 2005) which have been widely used in analyses of this kind. During OND, the easterly steering flow anomalies become even stronger, while the La Niña-like SST anomalies prevail in the tropical central and eastern Pacific (Figure 9d).

The impacts of ENSO on steering flow have been widely discussed in the literature (e.g., Camargo et al. 2007; Kossin et al. 2010; Colbert and Soden 2012; Wang et al. 2014; Li et al. 2015). A typical Matsuno-Gill-type (Matsuno 1966; Gill 1980) response of the atmosphere can be induced over the tropical Atlantic and there is a weakening of the North Atlantic Subtropical High causing anomalous cyclonic flow in the eastern mid-Atlantic during El Niño (La Niña) seasons, which is conductive to less (more) TC landfalls (e.g., Colbert and Soden 2012; Kossin et al. 2010; Li et al. 2015). ENSO events, especially those in the central Pacific, are strongly associated with Pacific-North American Pattern (PNA) (e.g., Ashok et al. 2007; Weng et al. 2007, 2009), which may also bridge the influences of PMM on steering flow.

Therefore, the steering flow anomalies during the positive and negative PMM phases support the time-lagged relationship between MAM PMM and ASO TC landfall. This is also supported by the TC genesis anomalies during the positive and negative PMM phases. The time-lagged association between MAM PMM and ASO TC landfall is therefore largely attributed to the changes in both genesis and steering flow.

4.2. Modeling Results Using FLOR

To further verify the impacts of PMM on TC landfall over the U.S. coast, we performed a set of perturbation experiments with GFDL FLOR, where SST is partially allowed to change. The SST anomalies associated with the positive PMM pattern moved from the subtropical eastern Pacific to tropical central Pacific in ASO (Figure 11). In ASO, the PPMM pattern (PPMM minus CTRL) produces the strongest SST warming in the tropical central Pacific (Figure 11a) while the SST warming was originally the strongest in the subtropical eastern Pacific in PPMM (Figure 11b). This suggests that the SST anomalies associated with PPMM tend to be followed by the central Pacific warming, which has been widely documented in the literature. Such tropical Pacific warming strongly modulates TC activity in the North Atlantic. Moreover, the TC density and genesis anomalies in PPMM minus CTRL experiments are strongly negative along the U.S. coast and in the North Atlantic (Figure 11), suggesting a suppression of TC landfall during ASO with positive PPMM. The steering flow anomalies in PPMM minus CTRL experiments are characterized by westerly and they are comparable with those in the observations (Figure 12). The westerly steering flow in PPMM minus CTRL experiments is consistent with less TC landfalls during the positive MAM PMM phase (Figure 12). The steering flow anomalies are consistent with the anomalous 200hPa geopotential height, which features a wave train propagating from the tropical Pacific to North America, similar to the PNA pattern. This suggests that the central Pacific warming may modulate TC landfall by triggering atmospheric teleconnections, which is also supported by previous findings showing that the central Pacific El Niño is strongly associated with the PNA pattern (e.g., Ashok et al. 2007; Weng et al. 2007, 2009).

5. Conclusions

Improved understanding of physical controls on North Atlantic TCs making landfall in the United States has been the subject of large interest by the scientific community because of the catastrophic effects that these storms can have. Here we have examined the role played by the PMM and its impact on U.S. landfalling TCs.

We have found that there is a statistically significant time-lagged association between MAM PMM and the ASO TC landfall activity over the U.S. coast, especially over the Gulf of Mexico and Florida. Specifically, the positive (negative) MAM PMM events tend to be followed by fewer (more) U.S. landfalling TCs in the following peak season. This lagged association is mainly caused by the lagged impacts of PMM on ENSO, and the subsequent impacts of ENSO on TC landfall. Positive (negative) PMM events are largely followed by El Niño (La Niña) events, which lead to less (more) TC geneses close to the U.S. coastline (i.e., the Gulf of Mexico and Caribbean Sea) and easterly (westerly) steering flow in the vicinity of the U.S. coast: these conditions are in turn unfavorable (favorable) for TC landfall over the Gulf of Mexico and Florida. Although concurrent (ASO) PMM has some impacts on the peak-season TC landfall activity, the impacts are weaker than the lagged impacts induced by MAM PMM.

The steering flow for TCs in the North Atlantic can be modulated by the Atlantic warm pool, the Atlantic Meridional Mode and ENSO (e.g., Kossin et al. 2010; Colbert and Soden, 2012; Wang et al. 2012). Moreover, the steering flow in the North Atlantic can also be modulated by the tropical Pacific SST forcing due to the Matsuno-Gill responses (Li et al. 2015). The PNA pattern may bridge the influences of the central Pacific El Niño on steering flow. The present study therefore provides insights into the impacts of the central Pacific warming on TC activity in the North Atlantic. Further analysis on the verification of such mechanisms underpinning changes in steering flow will be the focus of our future study.

326 The time-lagged impacts of MAM PMM on TC landfall provide the scientific and operational
327 community with a new quantity that can be potentially useful to forecast the seasonal frequency
328 of U.S. landfalling TCs, especially over the Gulf of Mexico and Florida. In addition, current
329 seasonal prediction model for TC landfall may be improved if PMM can be satisfactorily predicted
330 by current climate models in boreal spring.
331
332 *Acknowledgments*. The authors acknowledge funding from the National Science Foundation under
333 grant No. AGS-1262099, and Award NA14OAR4830101 from the National Oceanic and
334 Atmospheric Administration, U.S. Department of Commerce.
335

References:

Anderson, B. T., 2003: Tropical Pacific sea-surface temperatures and preceding sea level pressure anomalies in the subtropical North Pacific. J. Geophys. Res, 108.

Anderson, B. T., 2004: Investigation of a large-scale mode of ocean-atmosphere variability and its relation to tropical Pacific sea surface temperature anomalies. Journal of climate, 17, 4089-4098.

Ashok, K., S. K. Behera, S. A. Rao, H. Weng, and T. Yamagata, 2007: El Niño Modoki and its possible teleconnection. J. Geophys. Res, 112, C11007.

Boschat, G., P. Terray, and S. Masson, 2013: Extratropical forcing of ENSO. Geophysical Research Letters, 40, 1605-1611.

Bove, M. C., J. J. O'Brien, J. B. Eisner, C. W. Landsea, and X. Niu, 1998: Effect of El Niño on US landfalling hurricanes, revisited. Bulletin of the American Meteorological Society, 79, 2477-2482.

Camargo, S. J., A. W. Robertson, S. J. Gaffney, P. Smyth, and M. Ghil, 2007: Cluster analysis of typhoon tracks. Part II: Large-scale circulation and ENSO. Journal of Climate, 20, 3654-3676.

Chan, J.C.L., and W. M. Gray, 1982: Tropical cyclone movement and surrounding flow relationships. Monthly Weather Review, 110, 1354-1374.

Chang, P., L. Ji, and H. Li, 1997: A decadal climate variation in the tropical Atlantic Ocean from thermodynamic air-sea interactions. Nature, 385, 516-518.

Chang, P., and Coauthors, 2007: Pacific meridional mode and El Niño—Southern Oscillation. Geophysical Research Letters, 34, L16608.

Chiang, J. C., and C. M. Bitz, 2005: Influence of high latitude ice cover on the marine Intertropical Convergence Zone. Clim Dyn, 25, 477-496.

Chiang, J. C. H., and D. J. Vimont, 2004: Analogous Pacific and Atlantic Meridional Modes of Tropical Atmosphere–Ocean Variability*. Journal of Climate, 17, 4143-4158.

Colbert, A. J., and B. J. Soden, 2012: Climatological variations in North Atlantic tropical cyclone tracks. Journal of climate, 25, 657-673.

Delworth, T. L., and Coauthors, 2012: Simulated Climate and Climate Change in the GFDL CM2.5 High-Resolution Coupled Climate Model. Journal of Climate, 25, 2755-2781.

Delworth, T. L., and Coauthors, 2006: GFDL's CM2 Global Coupled Climate Models. Part I: Formulation and Simulation Characteristics. Journal of Climate, 19, 643-674.

Deser, C., and J. M. Wallace, 1987: El Niño events and their relation to the Southern Oscillation: 1925–1986. Journal of Geophysical Research: Oceans, 92, 14189-14196.

Di Lorenzo, E., G. Liguori, N. Schneider, J. Furtado, B. Anderson, and M. Alexander, 2015: ENSO and meridional modes: A null hypothesis for Pacific climate variability. Geophysical Research Letters, 42, 9440-9448.

Ding, R., J. Li, Y. h. Tseng, C. Sun, and Y. Guo, 2015: The Victoria mode in the North Pacific linking extratropical sea level pressure variations to ENSO. Journal of Geophysical Research: Atmospheres, 120, 27-45.

Elsner, J. B., 2003: Tracking hurricanes. Bulletin of the American Meteorological Society, 84, 353-356.

Elsner, J. B., and T. H. Jagger, 2006: Prediction models for annual US hurricane counts. Journal of Climate, 19, 2935-2952.

Emanuel, K. A., and D. S. Nolan, 2004: Tropical cyclone activity and the global climate system. Preprints, 26th Conf. on Hurricanes and Tropical Meteorology, Miami, FL, Amer. Meteor. Soc. A.

Gill, A. E., 1980: Some simple solutions for heat-induced tropical circulation. Quarterly Journal of the Royal Meteorological Society, 106, 447-462.

Kalnay, E., et al. (1996), The NCEP/NCAR 40-Year Reanalysis Project, Bulletin of the American Meteorological Society, 77(3), 437-471.

Kim, H.-M., P. J. Webster, and J. A. Curry, 2010: Modulation of North Pacific Tropical Cyclone Activity by Three Phases of ENSO. Journal of Climate, 24, 1839-1849.

Kim, S. T., J.-Y. Yu, A. Kumar, and H. Wang, 2012: Examination of the two types of ENSO in the NCEP CFS model and its extratropical associations. Monthly Weather Review, 140, 1908-1923.

Kirtman, B. P., et al., 2014: The North American Multimodel Ensemble: Phase-1 Seasonal-to-Interannual Prediction; Phase-2 toward Developing Intraseasonal Prediction. Bulletin of the American Meteorological Society 95(4): 585-601.

Klotzbach, P. J., 2011: El Niño-Southern Oscillation's impact on Atlantic basin hurricanes and US landfalls. Journal of Climate, 24, 1252-1263.

Kossin, J. P., S. J. Camargo, and M. Sitkowski, 2010: Climate modulation of North Atlantic hurricane tracks. Journal of Climate, 23, 3057-3076.

Kug, J.-S., F.-F. Jin, and S.-I. An, 2009: Two Types of El Niño Events: Cold Tongue El Niño and Warm Pool El Niño. Journal of Climate, 22, 1499-1515.

Landsea, C. W., and J. L. Franklin, 2013: Atlantic Hurricane Database Uncertainty and Presentation of a New Database Format. Monthly Weather Review, 141, 3576-3592.

Larson, S., S. K. Lee, C. Wang, E. S. Chung, and D. Enfield, 2012: Impacts of non‐canonical El Niño patterns on Atlantic hurricane activity. Geophysical Research Letters, 39.

Larson, S. M., and B. P. Kirtman, 2014: The Pacific Meridional Mode as an ENSO Precursor and Predictor in the North American Multimodel Ensemble. Journal of Climate, 27, 7018-7032.

Lee, S.-K., C. Wang, and D. B. Enfield, 2010: On the impact of central Pacific warming events on Atlantic tropical storm activity. Geophys. Res. Lett., 37, L17702.

Li, W., L. Li, and Y. Deng, 2015: Impact of the Interdecadal Pacific Oscillation on Tropical Cyclone Activity in the North Atlantic and Eastern North Pacific. Scientific Reports, 5, 12358.

Lin, C. Y., J. Y. Yu, and H. H. Hsu, 2015: CMIP5 model simulations of the Pacific meridional mode and its connection to the two types of ENSO. International Journal of Climatology, 35, 2352-2358.

Marks, F. D., and L. K. Shay, 1998: Landfalling tropical cyclones: Forecast problems and associated research opportunities. Bulletin of the American Meteorological Society, 79, 305-323.

Matsuno, T., 1966: Quasi-geostrophic motions in the equatorial area. J. Meteor. Soc. Japan, 44, 25-43.

Murakami, H., G.A. Vecchi, G. Villarini, T. Delworth, R. Gudgel, S. Underwood, X. Yiang, W. Zhang, and S.-J. Lin, Seasonal forecasts of major hurricanes and landfalling tropical cyclones using a high-resolution GFDL coupled climate model, Journal of Climate, 2016 (in press).

Patricola, C. M., P. Chang, and R. Saravanan, 2016: Degree of simulated suppression of Atlantic tropical cyclones modulated by flavour of El Niño. Nature Geoscience, 9, 155-160.

Pegion, K., and M. Alexander, 2013: The seasonal footprinting mechanism in CFSv2: simulation and impact on ENSO prediction. Clim Dyn, 41, 1671-1683.
Pielke Jr, R., and C. Landsea, 1999: La Niña, El Niño, and Atlantic hurricane damages in the United States. Bulletin of the American Meteorological Society, 80, 2027-2033.
Pielke Jr, R., J. Gratz, C. Landsea, D. Collins, M. Saunders, and R. Musulin, 2008: Normalized hurricane damage in the United States: 1900–2005. Natural Hazards Review, 9, 29.
Rayner, N., and Coauthors, 2003: Global analyses of sea surface temperature, sea ice, and night marine air temperature since the late nineteenth century. J. Geophys. Res, 108, 4407.
Saunders, M. A., and A. S. Lea, 2005: Seasonal prediction of hurricane activity reaching the coast of the United States. Nature, 434, 1005-1008.
Smith, A. B., and R. W. Katz, 2013: US billion-dollar weather and climate disasters: data sources, trends, accuracy and biases. Nat Hazards, 67, 387-410.
Smith, S. R., J. Brolley, J. J. O'Brien, and C. A. Tartaglione, 2007: ENSO's Impact on Regional U.S. Hurricane Activity. Journal of Climate, 20, 1404-1414.
Vecchi, G. A., and G. Villarini, 2014: Next season's hurricanes. Science, 343, 618-619.
Vecchi, G. A., and Coauthors, 2014: On the Seasonal Forecasting of Regional Tropical Cyclone Activity. Journal of Climate, 27, 7994-8016.
Velden, C. S., C. M. Hayden, W. Paul Menzel, J. L. Franklin, and J. S. Lynch, 1992: The impact of satellite-derived winds on numerical hurricane track forecasting. Weather and forecasting, 7, 107-118.
Villarini, G., G. A. Vecchi, and J. A. Smith, 2011: U.S. Landfalling and North Atlantic Hurricanes: Statistical Modeling of Their Frequencies and Ratios. Monthly Weather Review, 140, 44-65.
Vimont, D. J., D. S. Battisti, and A. C. Hirst, 2001: Footprinting: A seasonal connection between the tropics and mid-latitudes. Geophysical Research Letters, 28, 3923-3926.
Vimont, D. J., J. M. Wallace, and D. S. Battisti, 2003: The Seasonal Footprinting Mechanism in the Pacific: Implications for ENSO*. Journal of Climate, 16, 2668-2675.
Wang, C., and S.-k. Lee, 2007: Atlantic warm pool, Caribbean low-level jet, and their potential impact on Atlantic hurricanes. Geophysical Research Letters, 34, n/a-n/a.
Wang, C., S. K. Lee, and D. B. Enfield, 2008: Atlantic warm pool acting as a link between Atlantic multidecadal oscillation and Atlantic tropical cyclone activity. Geochemistry, Geophysics, Geosystems, 9.
Wang, C., H. Liu, S.-K. Lee, and R. Atlas, 2011: Impact of the Atlantic warm pool on United States landfalling hurricanes. Geophysical Research Letters, 38, n/a-n/a.
Wang, H., and Coauthors, 2014: How well do global climate models simulate the variability of Atlantic tropical cyclones associated with ENSO? Journal of Climate, 27, 5673-5692.
Weng, H., S. K. Behera, and T. Yamagata, 2009: Anomalous winter climate conditions in the Pacific rim during recent El Niño Modoki and El Niño events. Clim Dyn, 32, 663-674.
Weng, H., K. Ashok, S. Behera, S. Rao, and T. Yamagata, 2007: Impacts of recent El Niño Modoki on dry/wet conditions in the Pacific rim during boreal summer. Climate Dynamics, 29, 113-129.
Xie, L., T. Yan, L. J. Pietrafesa, J. M. Morrison, and T. Karl, 2005: Climatology and Interannual Variability of North Atlantic Hurricane Tracks. Journal of Climate, 18, 5370-5381.
Xie, S.-P., and S. G. H. Philander, 1994: A coupled ocean-atmosphere model of relevance to the ITCZ in the eastern Pacific. Tellus A, 46, 340-350.

Zhang, L., P. Chang, and L. Ji, 2009a: Linking the Pacific Meridional Mode to ENSO: Coupled Model Analysis. Journal of Climate, 22, 3488-3505.
Zhang, L., P. Chang, and M. K. Tippett, 2009b: Linking the Pacific meridional mode to ENSO: Utilization of a noise filter. Journal of Climate, 22, 905-922.
Zhang, W., G. A. Vecchi, H. Murakami, G. Villarini, and L. Jia, 2016: The Pacific Meridional Mode and the Occurrence of Tropical Cyclones in the Western North Pacific. Journal of Climate, 29, 381-398.

Table 1. Correlation coefficients between PMM in March to May (MAM), June to August (JJA) and August to October (ASO) and the frequency of U.S. landfalling TCs over different coastal regions (1948–2015). The symbol "*" represents the correlation coefficients which are significant at the 0.05 significance level. "Gulf & Florida" represents TCs that made landfall over the Gulf of Mexico and Florida combined.

Correlation	**Gulf**	**Florida**	**Gulf & Florida**	**Southeast**	**Northeast**	**US Coast**
PMM (MAM)	**-0.26***	**-0.35***	**-0.36***	-0.20	-0.15	**-0.32***
PMM (JJA)	-0.06	-0.20	-0.15	-0.06	-0.04	-0.12
PMM (ASO)	-0.13	-0.22	-0.20	-0.10	-0.007	-0.15

Table 2. List of the ten years with the strongest positive and negative MAM PMM values during the 1948-2015 period.

PMM Phases	Years
Positive PMM	1954, 1959, 1966, 1967, 1968, 1980, 1986, 1994, 1995, 2015
Negative PMM	1975, 1976, 1983, 1998, 1999, 2000, 2001, 2008, 2011, 2012

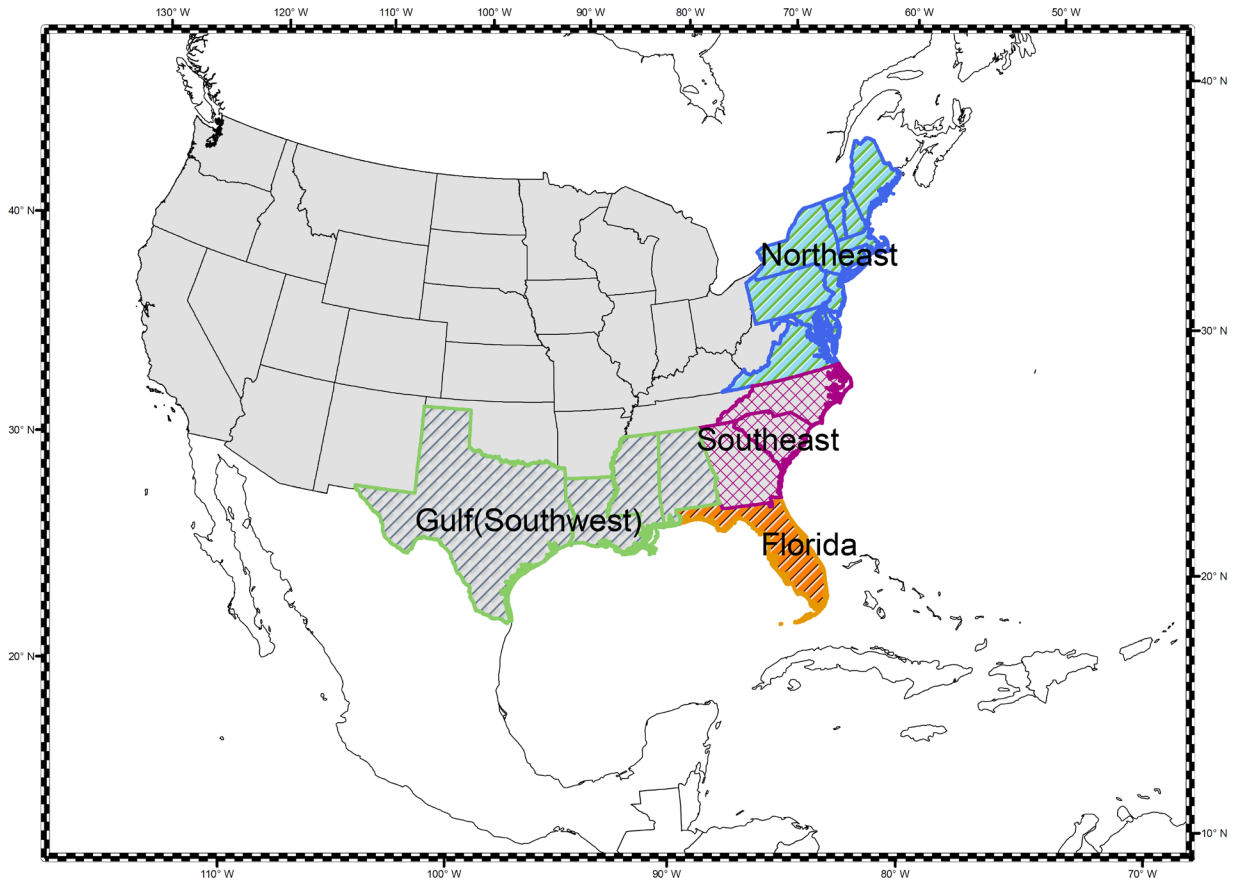

Figure 1. The four coastal regions used to define TC landfall including Southwest (Gulf of Mexico, green), Florida (orange), Southeast (purple) and Northeast (blue).

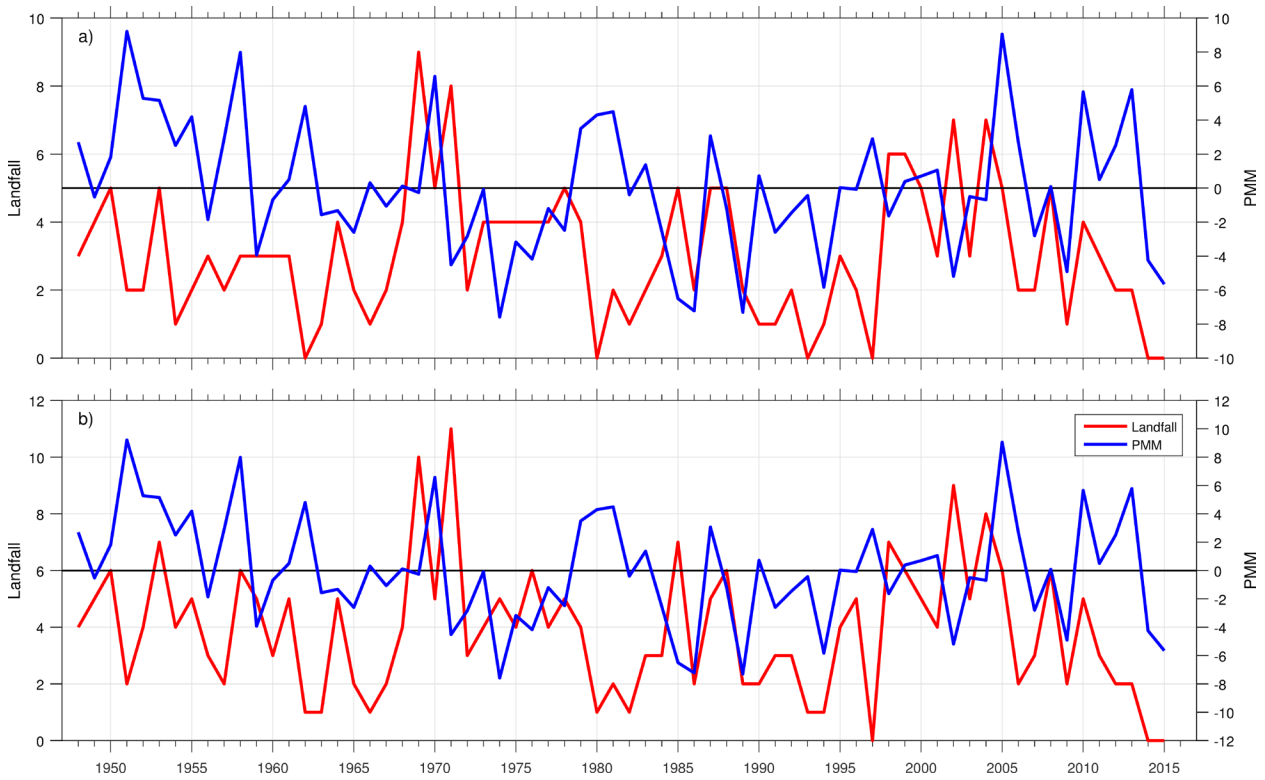

Figure 2. Time series of the MAM PMM index and the number of landfalling TCs during the August-October period. Panel a refers to the storms making landfall along the Gulf of Mexico and Florida (correlation coefficient of -0.36), while panel b to the number of storms making landfall along the U.S. coastline (correlation coefficient of -0.32).

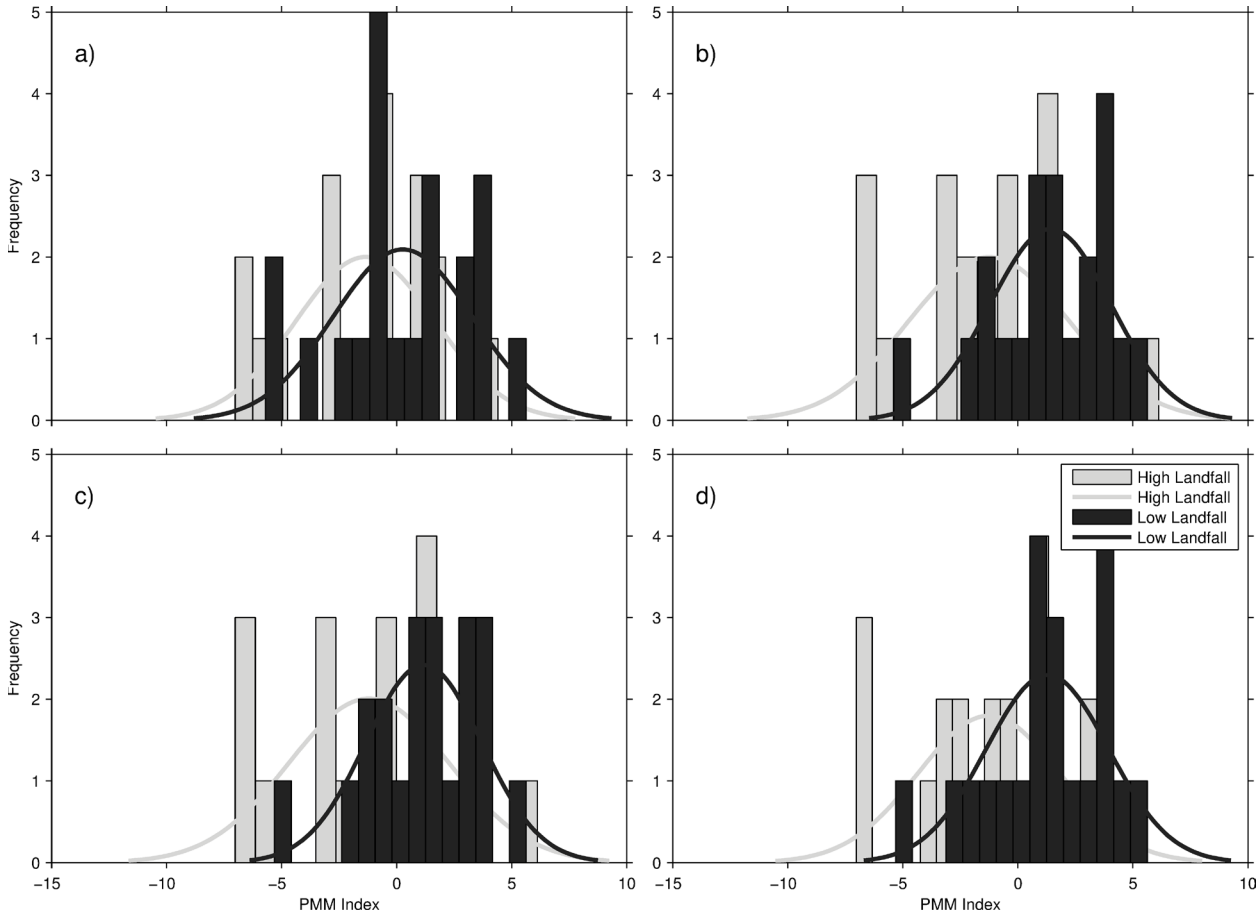

Figure 3. Histogram and fitted Gaussian distribution of the MAM PMM indices when the frequency of landfalling TCs during ASO is the highest (grey) or the lowest (black) over (a) Gulf, (b) Florida, (c) Gulf of Mexico and Florida, and (d) the entire U.S. coast.

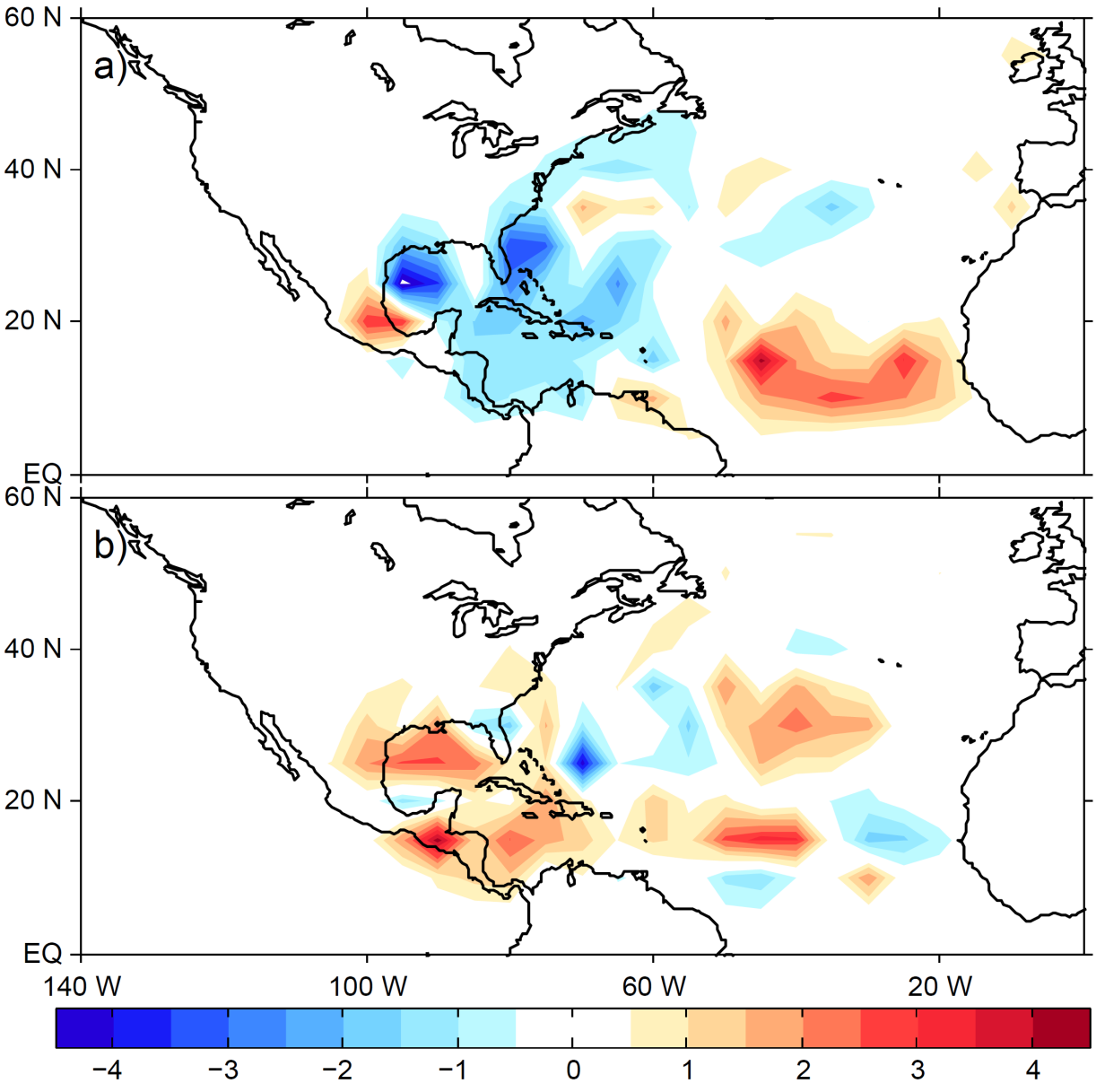

Figure 4. ASO TC track density anomalies (shading, unit: occurrences/season) when MAM PMM is (a) positive and (b) negative. Hurricane track density is calculated by binning hurricane tracks into 5° × 5° grid boxes. The base period for climatology is 1948-2015.

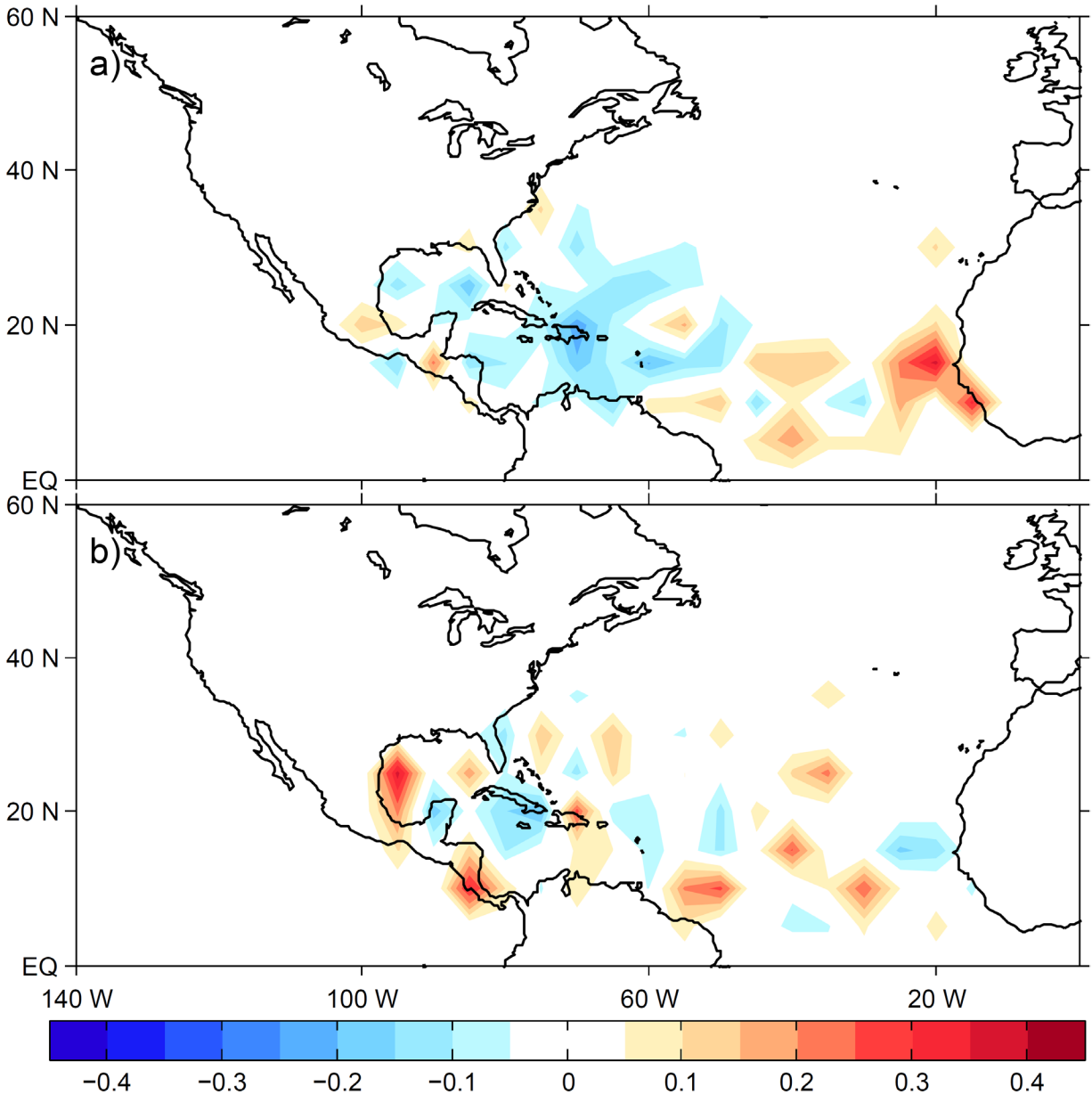

Figure 5. ASO TC genesis density anomalies (shading, unit: occurrences/season) when MAM PMM is (a) positive and (b) negative. TC genesis density is calculated by binning the storm tracks into 5° × 5° grid boxes. The base period for climatology is 1948-2015.

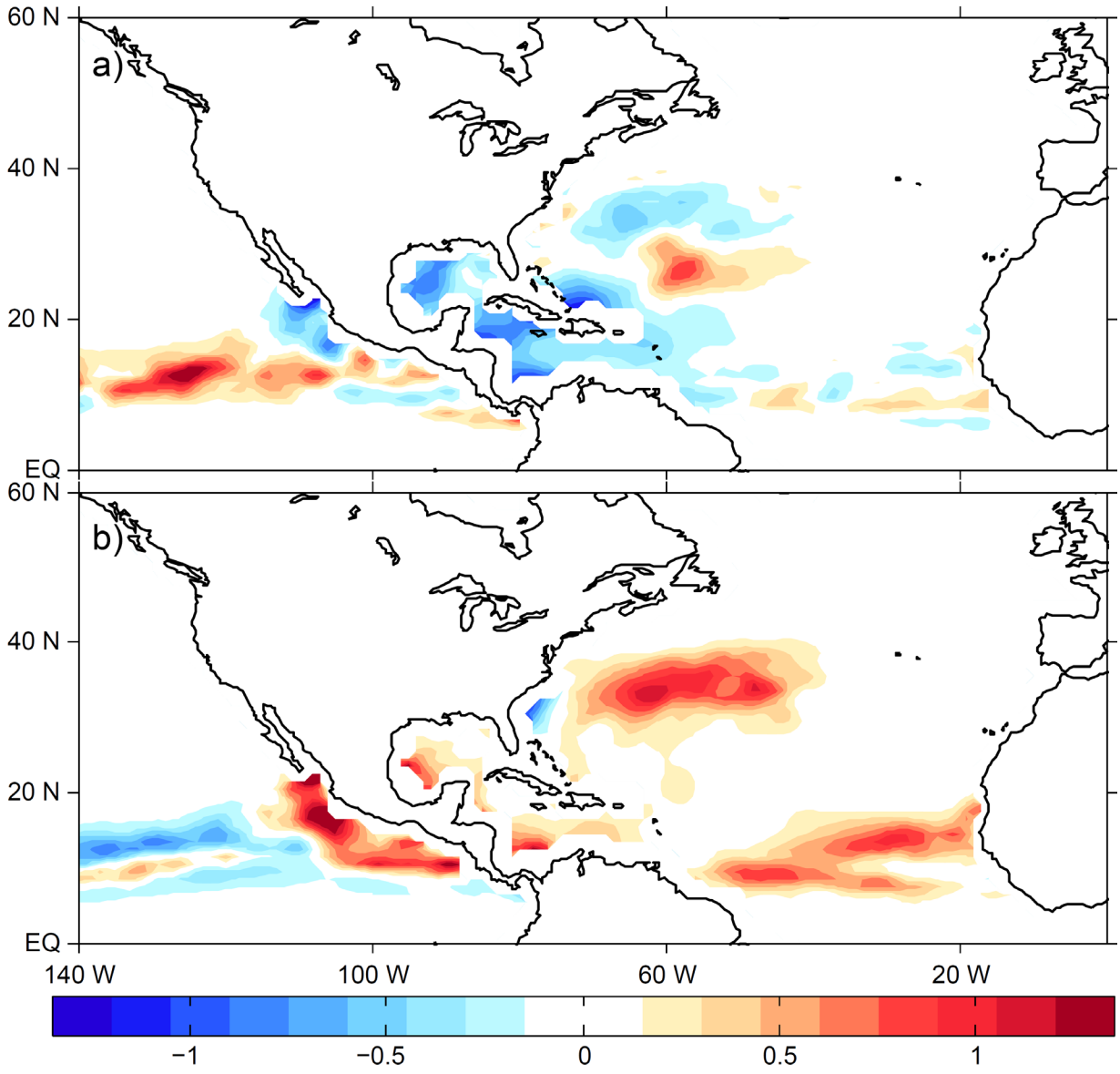

Figure 6. ASO TC genesis potential index anomalies (shading, unit: occurrences/season) when MAM PMM is (a) positive and (b) negative.

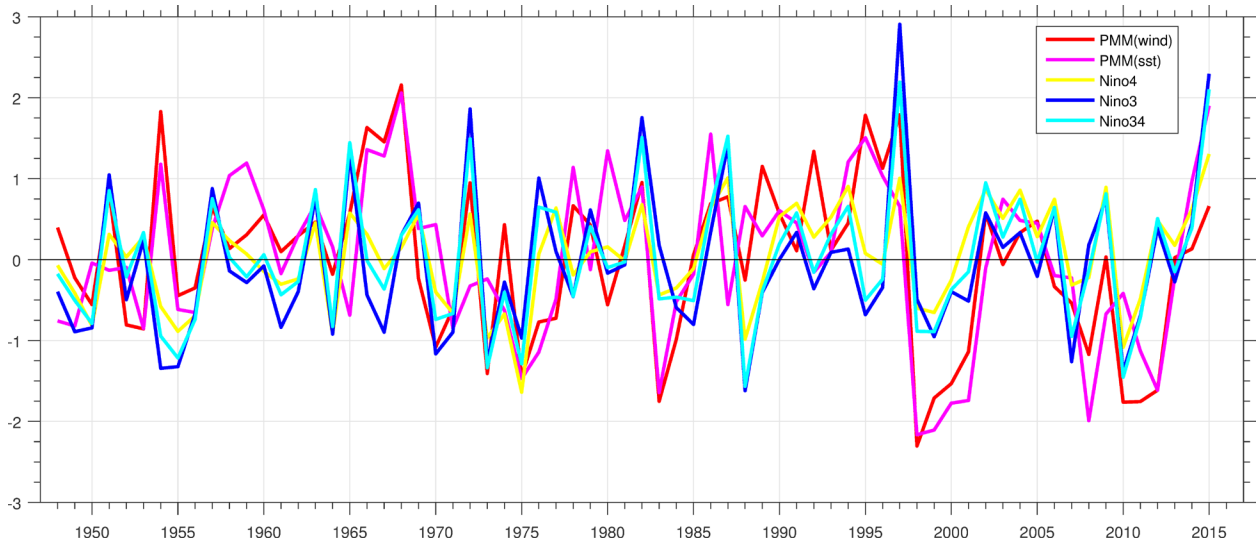

Figure 7. Time series of PMM (wind and SST) in March-May (red and magenta, respectively), and Niño4 (yellow), Niño3 (blue), Niño3.4 (cyan) indices averaged over the August-October for the period 1948-2105. The PMM index (wind and SST) is normalized.

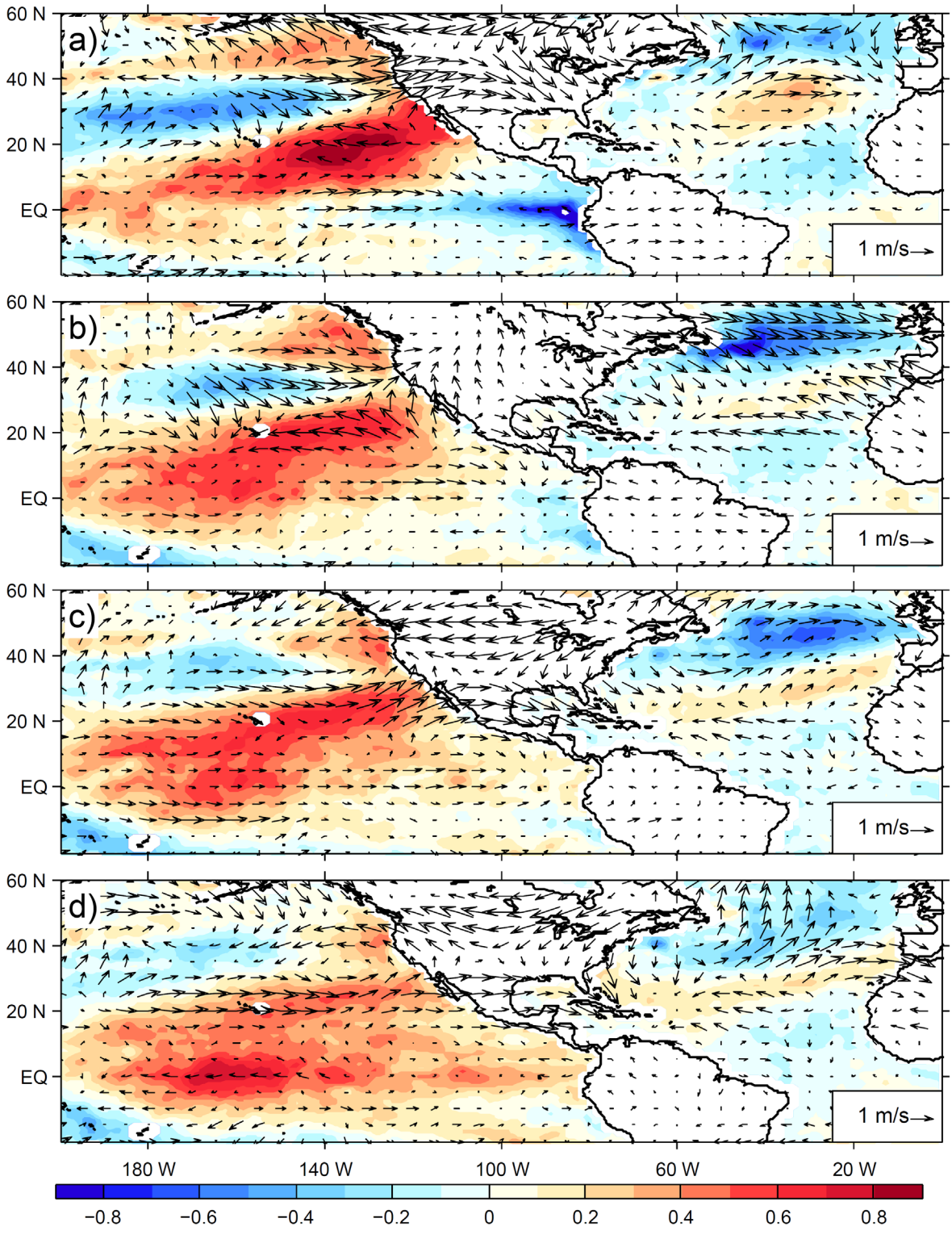

Figure 8. Composite SST (shading, unit: ºC; see color bar) and steering flow (wind vectors) anomalies during MAM, JJA, ASO, and OND when the MAM PMM is in the positive phase.

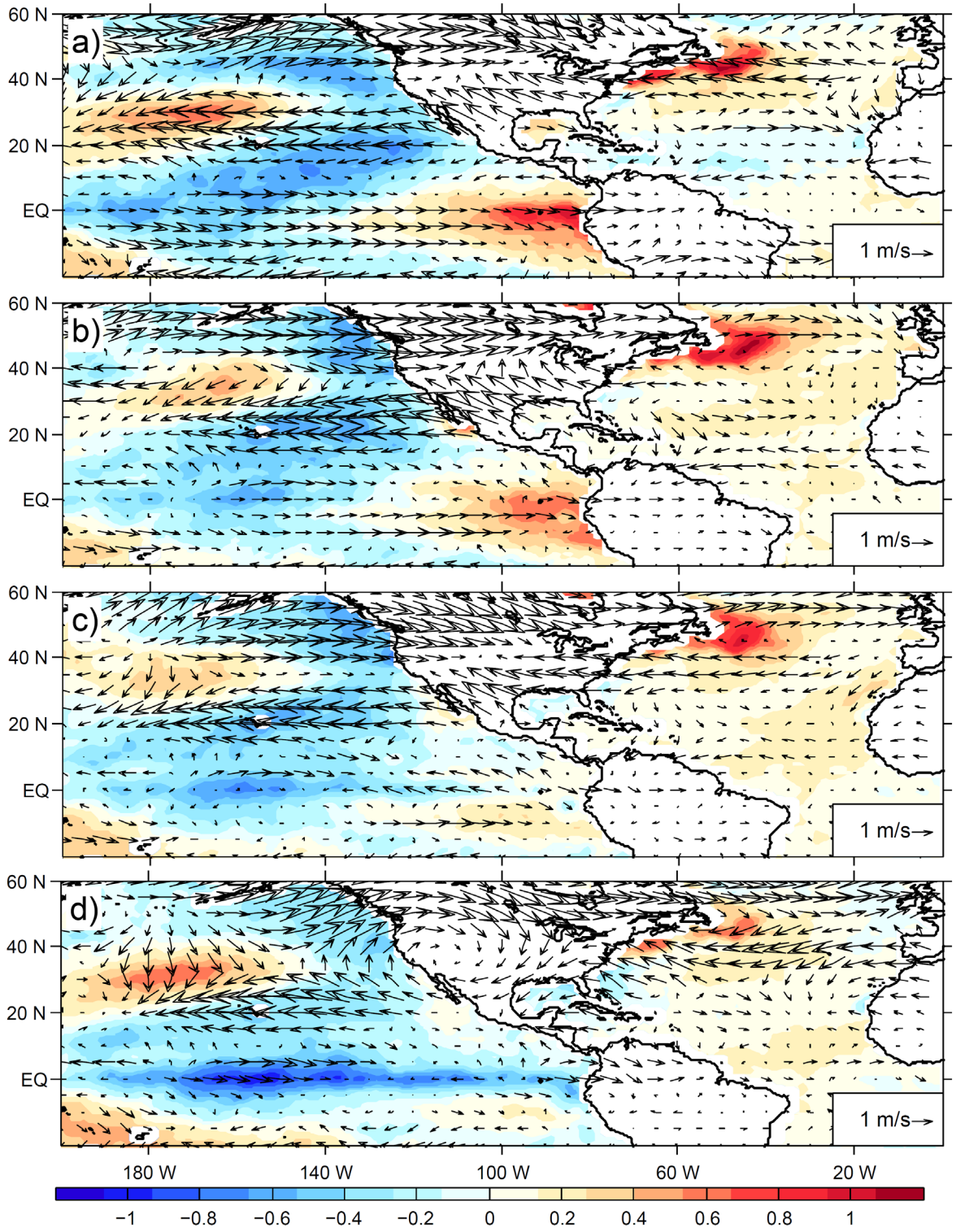

Figure 9. Same as Figure 8 but for the negative MAM PMM years.

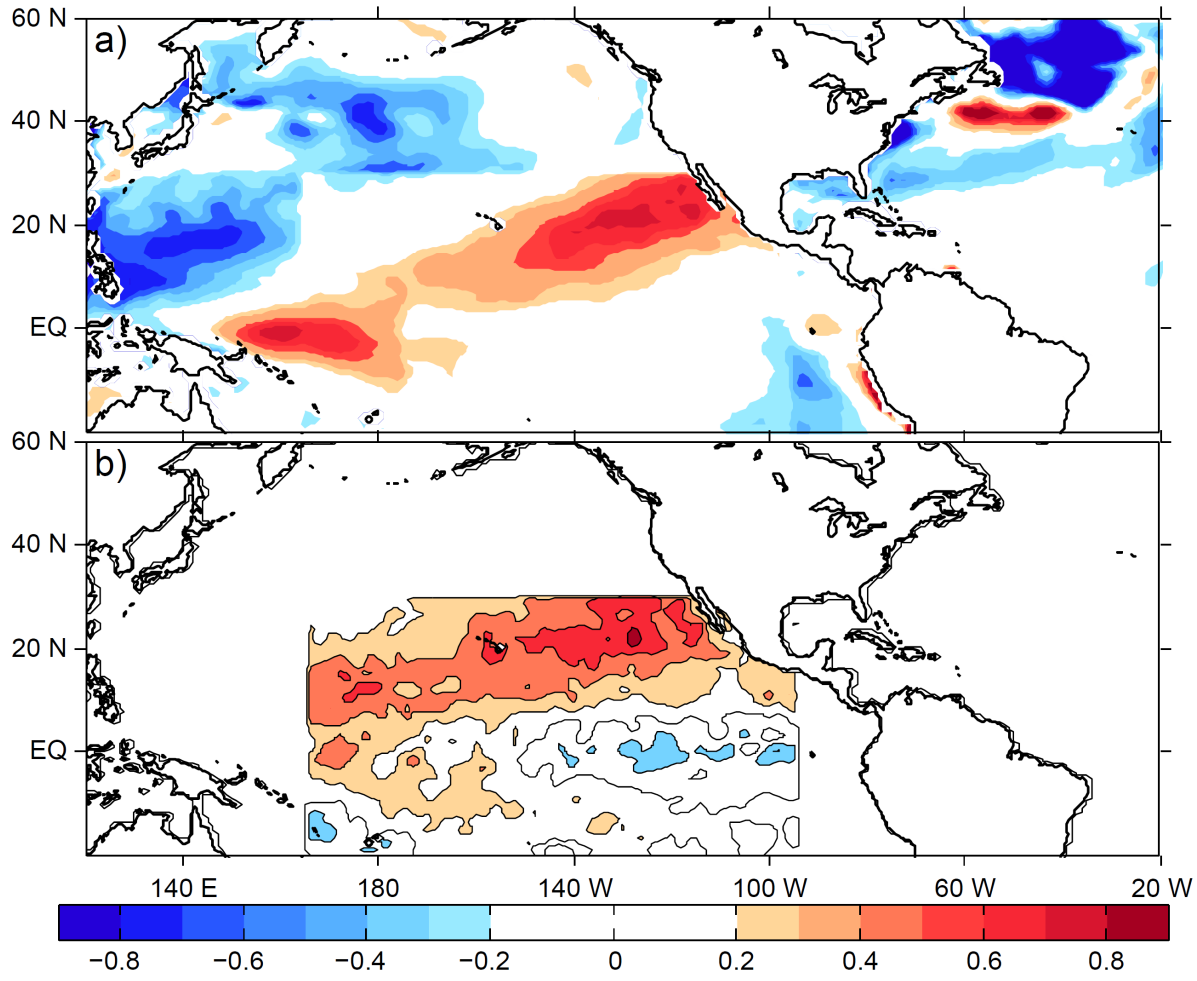

Figure 10. (a) Simulated SST anomalies in (shading, unit: ºC) in PPMM minus CTRL experiments (ASO) and (b) the positive PMM pattern used in the PPMM experiment.

548

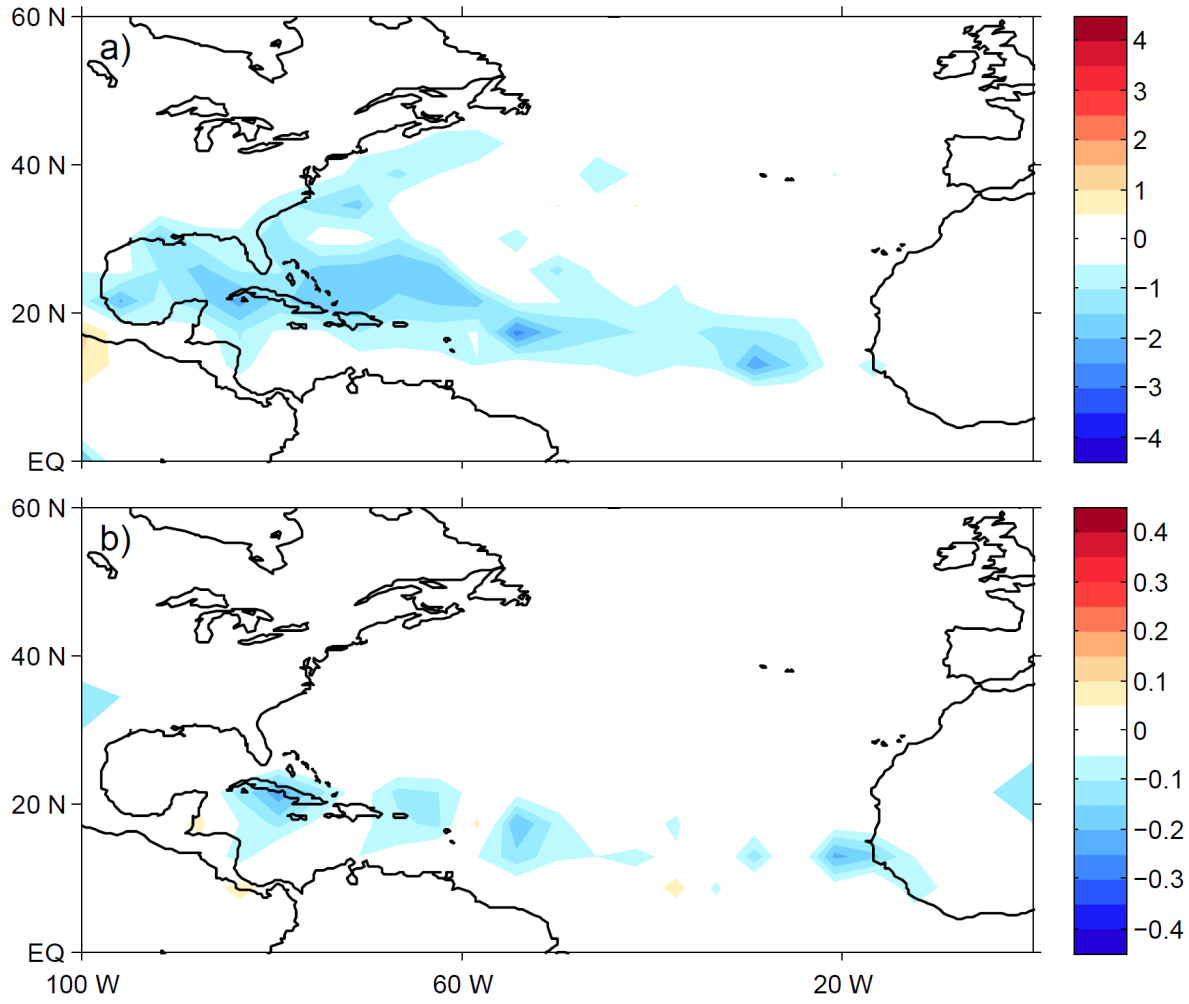

549
550

551 Figure 11. Responses of North Atlantic TC (a) density (shading, unit: occurrences/season) and (b)

552 genesis (shading, unit: occurrences/season) to the positive PMM (PPMM minus CTRL) in FLOR

553 experiments.

554

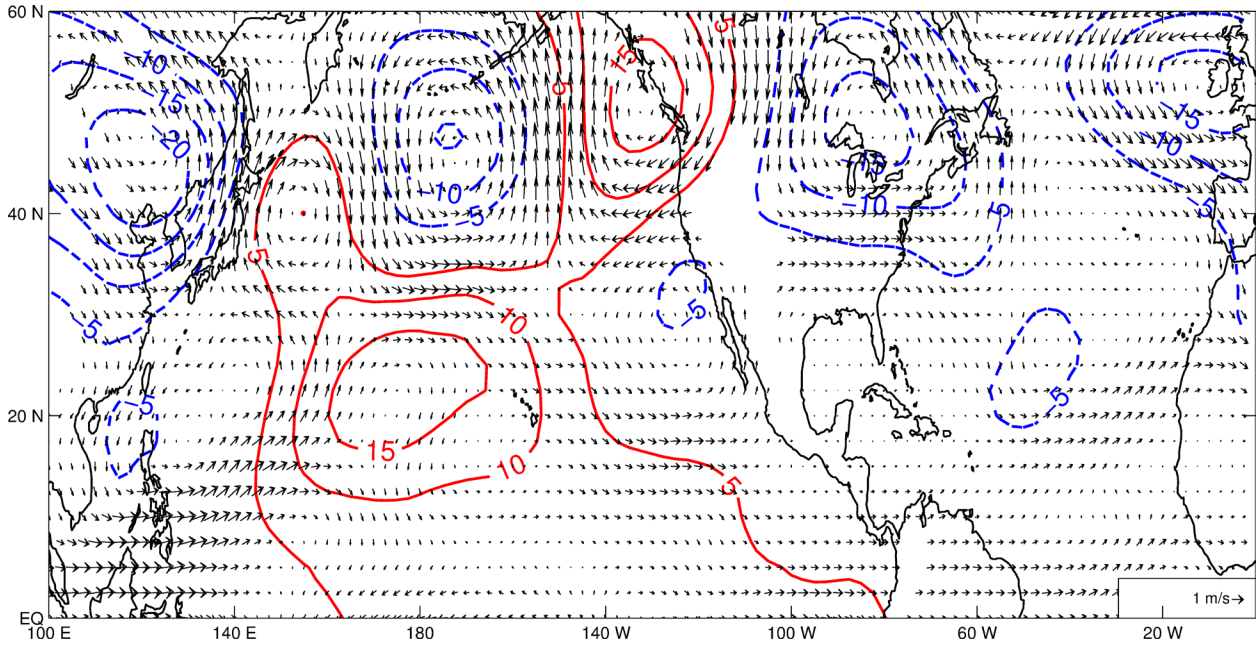

Figure 12. Responses of steering flow (vector, unit:ms^{-1}) and 200-hPa geopotential height (contours, unit: gpm) to positive PMM (PPMM minus CTRL) in FLOR experiments.